Miniaturized Diaphragm Vacuum Pump by Multi-Material Additive Manufacturing

Anthony P. Taylor and Luis Fernando Velásquez-García, *Senior Member, IEEE*

***Abstract*— This paper reports the first demonstration of a multi-material, fully additively manufactured, miniature diaphragm pump for creation and maintenance of low vacuum from atmospheric conditions. Using polyjet 3-D printing technology with 42 μm XY pixelation and 16 μm or 25 μm tall voxels, a single-stage vacuum pump design with active valves that has a total pumping volume of 1 cm^3 with 5% dead volume was implemented. Optimization of the devices resulted in manufacturing different constitutive parts of the pump in flexible materials of different stiffness. Finite element simulations of the pump design estimate at 0.20 MPa the maximum stress on the piston diaphragm root at full actuation, and at 106 Hz the natural frequency of the compression chamber. While operating at 1.82 Hz, the devices consistently pumped down from atmospheric pressure to 110 Torr in under 4 s, which is the smallest and fastest base pressure reported in the literature for a microfabricated diaphragm vacuum pump. In addition, the pumps can deliver mass flow rates as high as 200 sccm at 535 Torr, which is much higher than any of the reported flow rates from a diaphragm vacuum pump manufactured with standard microfabrication. The outgassing rate of the TangoBlack Plus® photopolymer used to print the pumps was measured and is on par with vacuum compatible elastomers. Compression chamber diaphragms exhibited lifetimes approaching 1 millioncycles, while the valves membranes have not leaked after over 2 million cycles. [2017-0100]**

***Index Terms*— 3-D printing of microsystems, diaphragm pump, polyjet printing, miniature vacuum pump, vacuum microelectromechanical systems (MEMS).**

I. Introduction

A VERY exciting research thrust in microtechnology is the development of microsystems that require a supply of gases at precise flow rates and pressure levels, e.g., miniaturized analytical instruments [1], [2]. These systems need vacuum pumps to operate, i.e., hardware that creates and maintains vacuum at a given flow rate. Miniaturized pumps that consume low power are needed to greatly extend the autonomy and deployability of these microsystems.

Positive displacement pumps exploit gas compressibility to create and maintain vacuum; they use active or passive valves to compress pockets of gas at low pressure to higher, e.g., atmospheric, pressure using a variable volume, i.e., compression chamber [3]. Positive displacement pumps are adequate for creating and supporting low vacuum (down to Torr level), and as roughing pump in combination with other kinds of pumps to reach lower pressure [4].

A diaphragm pump is a kind of positive displacement pump where the changes in volume of the compression chamber are caused by the displacements of a flexible membrane. Several research groups have investigated the miniaturization of diaphragm vacuum pumps using microfabrication. For example, Zhou et al. demonstrated a pneumatically-actuated, single-stage pump made of a silicon and glass wafer stack that reached a 164 Torr base pressure [5], which is until this work the highest reported vacuum from a MEMS membrane pump creating vacuum from atmospheric pressure. Also, Kim et al. demonstrated an electrostatically actuated 18-stage pump that produced an air flow rate of 4.0 sccm and maximum pressure drop of 17.5 kPa (∼130 Torr) [6]. In addition, Besharatian et al. reported an electrostatically actuated 24-stage pump in honeycomb arrangement that produced an air flow rate of 0.36 sccm and maximum pressure drop of 4.4 kPa (∼33 Torr). In general, the reported microfabricated pumps present a number of issues including (i) small pressure drops due to their large dead volume compared to the total pump volume, (ii) small flow rates due to the large hydraulic resistances of the hydraulic network, small compression chambers actuated at a slow pace, and sometimes significant valve leak rate, and (iii) expensive and time consuming manufacture, which makes them incompatible with low-cost applications.

Additive manufacturing (AM) is a set of layer-by-layer fabrication techniques that create solid objects using as template a computer-aided design (CAD) file [8]. Compared to standard microfabrication, AM offers advantages such as rapid prototyping, device customization, definition of freeform geometries, and broader material selection, while attaining minimum feature sizes on par with microfluidic systems (typical layer height is in the 10-300 μm range and typical XY voxel size is in the 25 – 500 μm range). In addition, a number of 3-D printing techniques make possible the definition of leak tight, closed channels or cavities; in particular, AM could create miniature diaphragm pumps with larger compression chamber displacements than what is achievable with standard microfabrication for better vacuum generation and larger flow rate. Several research groups have reported 3-D printed microfluidic devices –including pumps for incompressible liquids; these microsystems perform on par or better than corresponding microfabricated hardware, or demonstrate

Manuscript received April 28, 2017; revised August 1, 2017; accepted August 18, 2017. Date of publication September 5, 2017; date of current version November 29, 2017. This work was supported in part by Edwards Vacuum. Subject Editor A. Luque. *(Corresponding author: Luis Fernando Velásquez–García.)*

A. P. Taylor is with Edwards Vacuum, Sanborn, NY 14132 USA, and also with the Massachusetts Institute of Technology, Cambridge, MA 02139 USA (e-mail: anthony.taylor@edwardsvacuum.com).

L. F. Velásquez-García is with Microsystems Technology Laboratories, Massachusetts Institute of Technology, Cambridge, MA 02139 USA (e-mail: Velasquez@alum.mit.edu).

Color versions of one or more of the figures in this paper are available online at http://ieeexplore.ieee.org.

Digital Object Identifier 10.1109/JMEMS.2017.2743020

designs that are unfeasible/hard to make with standard microfabrication [9]–[15].

Most of the reported work on additively manufactured microfluidics is focused on one-material devices, that is, where all the components of the device are made of the same constitutive material [9], [10] –even in devices with monolithically integrated actuators, e.g., valves [12]. The one-material category includes devices made of a constitutive material and a sacrificial material (e.g., when defining closed channels by filling-in voxels with a dissolvable material encased in a non-dissolvable material) because the use of a second material reflects shortcomings of the manufacturing technique instead of adding functionality to the printed object. It would be highly desirable to tailor the constitutive material of each component of the device because each component is intended to efficiently satisfy specific requirements. For example, making rigid parts made of a stiff material connected to compliant parts made of a flexible material allows for implementing freeform long-stroke actuators –analogous to the way a bone structure is actuated by muscles in a vertebrate organism. At large, the manufacture of these multi-material 3-D printed MEMS should be carried out monolithically to obviate issues with post-assembly of the microsystem, e.g., component-to-component alignment; in particular, polyjet technology (roughly speaking, inkjet printing of UV curable, liquid printable feedstock [16]) is a mature AM method capable of monolithically printing an object where each voxel is made of a flexible material of different stiffness [17].

This paper reports the first multi-material, additively manufactured, miniaturized diaphragm pump in the literature. The valves and the compression chamber of these devices are made of flexible material with different stiffness, greatly extending performance and lifetime compared to our initial results of 3-D printed miniature diaphragm pumps using a single material [18]. Section II explains the considerations for selecting the printing method and printable feedstock, describes the metrology of vertical resolution structures, and reports the characterization of the surface topography, Young's modulus, and vacuum outgassing performance of the printable feedstock. Section III describes the design and fabrication of the mini pumps. Section IV describes the apparatus and experimental procedure, while Section V discusses the experimental results and proposes directions for future research. Section VI summarizes the work.

II. Selection and Characterization of AM Method

The ability to 3-D print flexible, thin, and leak tight membranes is essential to implement a diaphragm vacuum pump. However, many of the 3-D printing technologies require further refinement to attain such specifications and/or improvement of the mechanical properties of the printable materials [19]. For manufacturing the pump, three 3-D printing methods with a high degree of maturity that could yield nonporous, solid structures with embedded channels were considered [20]: (i) fused filament fabrication (FFF), i.e., an additive manufacturing method that creates layer by layer freeform solids by extruding a thermoplastic filament; (ii) digital light processing stereolithography (DLP-SLA), i.e., an additive manufacturing method that creates layer by layer freeform solids using a bath of UV-sensitive resin; and (iii) polyjet printing, i.e., an additive manufacturing method similar to inkjet printing that creates layer by layer freeform solids by UV curing droplets of liquid photopolymer that are jetted on a build tray. Flexible and thin membranes can be 3-D printed by the FFF method; however, an earlier version of our pump design made of the Ninjaflex® thermoplastic polymer [21] did not have leak tight membranes. We also investigated using DLP-SLA to print the pumps because microfluidic valves made by this method with up to 1-million cycles have been reported [12]; however, the maximum reported elongation of the photopolymers used in DLP-SLA is not as large as that of the flexible materials available for the polyjet method, which limits the ultimate pressure that can be attained by the diaphragm vacuum pump as it depends on the compression ratio of its chamber. In particular, while a maximum elongation of ∼85% can be achieved by the DLP-SLA-printable material FLFLGR02 [22], up to 220% of maximum elongation can be achieved by the polyjet-printable material TangoBlack Plus® with a Shore hardness of 27A [23]. Therefore, TangoBlack® –a family of acrylate-based UV curable photopolymers commercially available for polyjet printing with large maximum elongation, was selected as printable feedstock for manufacturing the miniature pumps; mixing different ratios of the base materials VeroClear® and TangoBlack Plus® results in printable feedstock with Shore hardness values between 27A and 95A [24].

A. Vertical Feature Resolution

In a diaphragm pump the vertical resolution of the manufacturing technique is very important because it strongly influences aspects such as the mechanical performance of the diaphragm and its leak rate. The vertical feature resolution of two variations of the printable material (Shore hardness of 27A and 50A) was investigated by comparing the correspondence between designed and printed test structures. Step pyramid test structures with step heights ranging between 208 μm and 8,416 μm were printed with a Polyjet Objet1000 Plus® printer (Stratasys, Eden Prairie, MN) using 16 μm tall voxels with 42 μm XY pixelation; metrology of the structures was conducted using a white light optical interferometer. Fig. 1 shows the measured height versus the designed (i.e., CAD) height of the steps printed in the TangoBlack Plus® (Shore 27A) and a TangoBlack® blend with Shore 50A hardness; each data point represents the averages of eight measurements or differences between measurements, for a total of eleven points for each material. The data demonstrate that there is a close match between the intended height and the printed height; linear best fits to the data have slopes within 3% (TangoBlack® blend) and 5% (TangoBlack Plus®) of the ideal 1-to-1 correspondence. In addition, a small offset (14 μm for TangoBlack® blend and 7 μm for TangoBlack Plus®) between measured and designed heights was observed; this offset is on the order of one slice, which is expected for an AM process.

B. Surface Topography Characterization

The surface topography of the printed material could influence the pump performance in two important aspects,

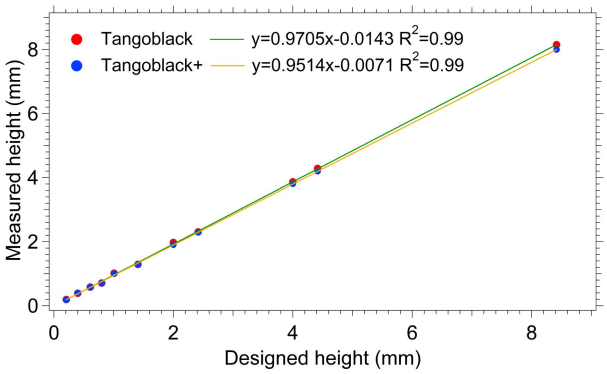

Fig. 1. Measured height versus CAD height of features on step pyramids 3-D printed in TangoBlack® and TangoBlack Plus® feedstock.

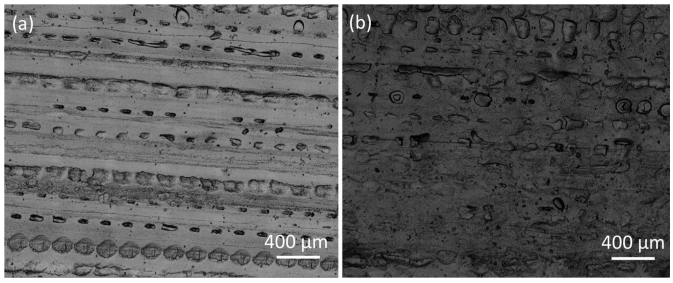

Fig. 2. Optical micrographs of a nominally flat surface made of (a) TangoBlack Plus® and (b) TangoBlack® blend with Shore hardness 50A.

TABLE I
ARITHMETIC ROUGHNESS (R_a) AND MAXIMUM TOP-TO-VALLEY HEIGHT (R_Z) OF NOMINALLY FLAT SURFACES

Sample	TangoBlack Plus®	TangoBlack® blend
Hardness	Shore 27A	Shore 50A
R_a (µm)	3.478	2.706
Standard dev. Ra (µm)	0.716	0.567
Rz (µm)	18.326	15.476
Standard dev. Rz (µm)	5.597	5.409

i.e., (i) helping create a leak tight seal between two surfaces, e.g., in the valves, and (ii) affecting the outgassing rate of the material. The surface texture of 3.2 mm by 4.4 mm nominally flat surfaces printed with 16 μm tall voxels and 42 μm XY pixelation in TangoBlack Plus® (Shore 27A) and TangoBlack® blend (Shore 50A) was characterized using a Keyence VK-X250 3D Laser Scanning Confocal Microscope with a 20X objective lens images; the data were analyzed using the standards ISO 4287 [25] and 4288 [26].

Optical micrographs of the surfaces are show in Fig. 2, while Table I is a summary of the estimated arithmetic roughness (R_a) and maximum top-to-valley height (R_z, *i.e.,* sum of largest roughness peak height and the largest roughness valley along a sampling length). The R_a values are on the order of a few microns, and the R_z values are close to the layer thicknesses (16 μm). In addition, Fig. 2 evidences striations in one direction with wavelength of about three XY pixels (~120 μm); we speculate that the striation is due to the arrangement in lines of the nozzles in the print head. In a stiff material, this topography could adversely affect the leak tightness of a seal between two surfaces; however, in a flexible and compliant material the topography helps seal the surface –this is analogous to the ridges in a human finger that facilitate object grasping [27].

C. Young's Modulus Characterization of TangoBlack® Blend With 50A Shore Hardness

Knowing the elastic properties of the printed material is essential to model the structural performance of the mini pump. The vendor of the polyjet-printable resins does not provide values of the Young's modulus for any of the TangoBlack® materials [24]; there are papers that report the Young's modulus for TangoBlack Plus® [27], [28], but to the best of the authors' knowledge there is no reported value for the TangoBlack® blend with 50A Shore hardness. Therefore, uniaxial tension tests where conducted with a PASCO Materials Testing Machine ME-8236 (Pasco, Roseville, CA) on ten printed coupons to characterize the Young's modulus of the 50A Shore TangoBlack®blend. The printed samples are flat strips of constant thickness with a central narrow portion with constant cross section; the coupons have a ridge on the top at both ends to interface with the flat coupon fixture Pasco ME-8238. During the test the pulling rate was constant, around 1.4 mm/min, and the sampling frequency was 2 Hz. From the tests, the Young's modulus of the TangoBlack® blend with 50A Shore hardness is estimated at 0.76 +/- 0.04 MPa (R^2 =0.99).

D. Vacuum Compatibility of TangoBlack Plus®

Characterization of the vacuum outgassing of the printable material was conducted to help answer three important questions, i.e., (i) whether the material outgassed at a rate that would affect the performance of the pump, (ii) the nature of the outgassed material, and (iii) how the outgassing of the material compared to the outgassing of typical vacuum-compatible polymers. The outgassing rate of a sheet made of TangoBlack Plus® was characterized using a 100 mm × 100 mm × 0.5 mm printed sample. The experimental apparatus is at Edwards Vacuum laboratories (Burgess Hill, UK) and is capable of generating 10^{-8} Torr base pressure and conducting mass spectrometry of the vacuum using a residual gas analyzer (RGA), detecting partial pressures as small as 10^{-14} Torr. Samples are placed in a wire mesh basket suspended in an ultra-high vacuum (UHV) compatible stainless steel chamber equipped with a 68 l/s turbomolecular pump and a Hiden Analytical 200 amu quadrupole mass spectrometer. Partial pressure measurements of gas species with masses ranging from 1 to 200 amu are acquired every ten minutes.

Fig. 3 is a plot of partial pressure versus atomic mass taken after 1, 10, and 145 hours of time in the chamber; the total outgassing rates (1-100 amu) along with values for water (18 amu) and hydrocarbons (45-100 amu and 101-200 amu) are listed in Table II. The calculated total outgassing rate

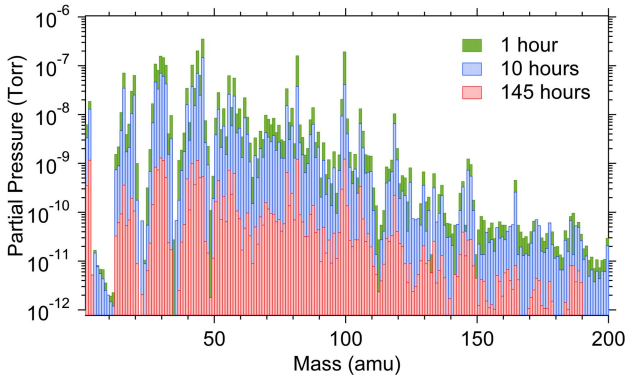

Fig. 3. Three partial pressure scans over 200 amu at 1,10, and 145 hours.

TABLE II
OUTGASSING MEASUREMENTS

	Mass Range	Rate, 1 hr	Rate, 10 hrs	Rate, 145 hrs
	amu	Torr.l/s.cm^2	Torr.l/s.cm^2	Torr.l/s.cm^2
TOTAL	1-100	2.9E-06	1.8E-06	1.8E-07
H_2O	18	3.5E-08	1.9E-08	1.6E-09
C_xH_y	45-100	1.3E-06	7.9E-07	8.8E-08
C_xH_y	101-200	6.1E-08	5.2E-08	1.4E-08

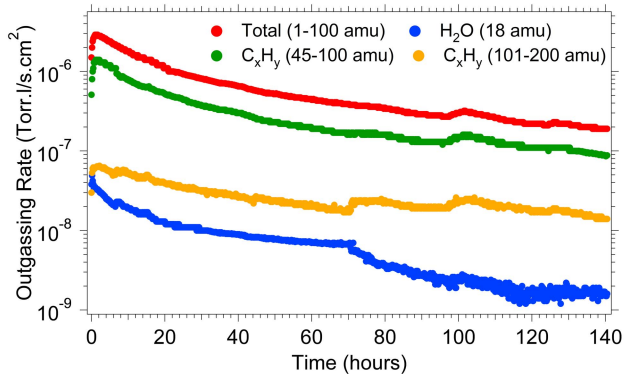

Fig. 4. The outgassing rate of TangoBlack Plus® decays over time.

of the sample at the 1- and 10-hour marks are in the range reported for common vacuum-compatible elastomers such as fluoroelastomer or Buna-N ($10^{-5} - 10^{-7}$ Torr.l/s.cm^2) [29]. Therefore, the performance of a diaphragm pump should not be significantly affected by the choice of a TangoBlack® resin as constitutive material; moreover, TangoBlack®-printed components, e.g., seal gaskets, should satisfactorily perform in vacuum. The large fraction of the total outgassing rate attributable to hydrocarbons with mass in the 45-100 amu range indicates the polymer sample tested might not have been fully cross-linked; we speculate that optimization of the layer-by-layer UV curing during the printing process might reduce the amount of hydrocarbon outgassing; this matter requires further study.

The evolution of the gas species over the 145-hour study is depicted in Fig. 4. During the first two hours the hydrocarbon outgassing rate increases while the water

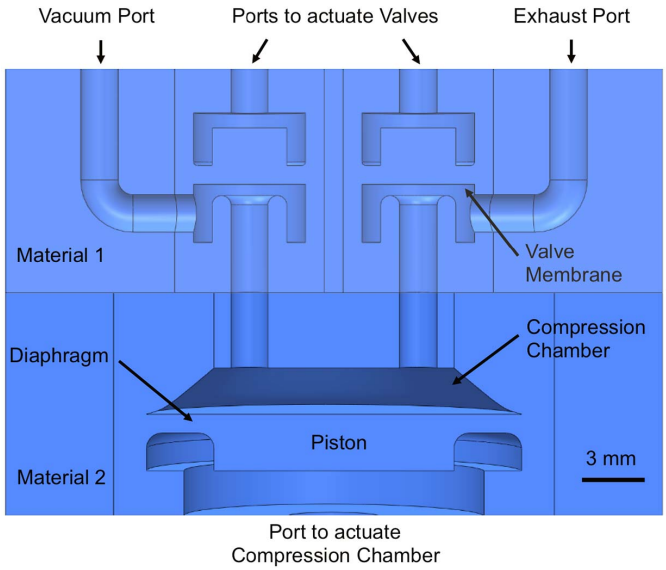

Fig. 5. CAD drawing of a cross-section of the diaphragm pump showing the compression chamber, valves, and fluidic ports; the cross-section cut passes through the centers of the valves and compression chamber. Different polymer blends may be used for the valve block (material 1) and the piston block (material 2). The dead volume of the pump is comprised of the two passageways between the compression chamber ceiling and the valve seats. During fabrication, the internal cavities of the pump are filled-in by a support material; after printing, the support material is removed with a 2% NaOH solution in H_2O and agitation.

outgassing rate decreases, suggesting there could be a capillary effect allowing trapped hydrocarbons to migrate to the surface. However, bursts in the outgassing rate of the hydrocarbon signatures after 70 and 100 hours of measurement suggest trapped gases are leaving the sample during these periods; this is quite possible due the granularity of the printed part, i.e., the printed object is made of discretized voxels stitched in air at atmospheric pressure. The continuous emission of hydrocarbon traces suggests that using a TangoBlack®-printed pump in a miniaturized analytical instrument could pose some challenges, e.g., the outgassing could increase the noise floor of the measurements.

III. DEVICE DESIGN AND FABRICATION

A CAD model of the additively manufactured single-stage miniature diaphragm vacuum pump is shown in Fig. 5 and an example of a monolithically printed pump is shown in Fig. 6. The pump consists of a compression chamber, two active valves, and the internal hydraulics that connect the valves, chamber, and ports; the device measures 28 mm wide by 35 mm long and 24 mm tall, and has a total pumping volume of 1 cm^3 with 5% dead volume. The pump creates vacuum by removing pockets of gas from a cavity, compressing them, and releasing them to a reservoir at atmospheric pressure. Active valves were chosen in this design because their timing can be set to optimize pump performance. The valves are pneumatically actuated; researchers have reported microfabricated valves with other means of actuation, e.g., piezoelectric [30], thermal (bimetallic) [31], and electrostatic [32]. Passive check valves were not explored, but they do offer the

Fig. 6. Example of a diaphragm pump 3-D printed in one piece of a TangoBlack® blend with Shore 50A hardness. The device was cut with a razor blade after printing and post-cleaning of the sacrificial material that filled-in the cavities.

advantage of not requiring additional energy and signals for actuation, and can be optimized to yield less dead volume than active valve pumps. There are reports of 3-D printed passive check valves [33]; however, passive check valves are limited in aspects such as the ratio between the forward and reverse pressure drop across the valve, the maximum operating pressure, and reliability [34].

The diaphragm pumps were polyjet 3-D printed in flexible photo-definable polymers of the TangoBlack® family using 42 μm-wide, 42 μm-long, and 25 or 16 μm-tall voxels; the printable support material FullCure® 705 temporarily filled-in the internal cavities of the pump during manufacturing. The support material was removed using a solution of 2% NaOH in H_2O and mechanical agitation; removal of the support material cannot be rushed; otherwise, the pumps could get damaged in the process. Although the pumps can be monolithically printed and the support material can be satisfactorily removed (e.g., in Fig. 6), printing the device in two monolithic blocks greatly facilitates the support material removal effort. In Fig. 5, the two blocks are shown in different hues; the blocks connect at the line drawn through the middle of the diagram. The lower half of the pump is the *piston block*, which contains the compression chamber and related internal hydraulics; the upper half is the *valve block,* which houses the vacuum and exhaust valves along with the inlet and outlet pipe network. Alignment of the block assembly is not critical because the two blocks meet at an interface with fairly large (2-mm diameter) features. The external top and bottom sides of the printed blocks are sticky to the touch and form a vacuum tight seal when placed in contact with each other, while being slightly compressed between the plates of the apparatus used to characterize the pumps (see Section IV). Arrangement of the four ports on top of the pump in a linear array with sufficient spacing allowed for using miniature brass pipe fittings barbed for ¼" tubing.

The in-plane dimensions of the 3-D printed mini pump and its components (Table III) are similar to those of the single-stage diaphragm MEMS pumps made with semiconductor microfabrication reported in [3] and [5], which also have exactly the same components. Specifically, the total

TABLE III
IN-PLANE DIMENSIONS OF COMPONENTS OF 3-D PRINTED VACUUM PUMP

Dimension	Value (mm)
Outer diameter compression chamber	20.0
Diameter compression chamber piston	12.8
Outer diameter valve	6.0
Diameter valve piston	4.0
Diameter valve ports	2.0

The radial dimension of the diaphragm of the compression chamber is 3.6 mm, and the radial dimension of the diaphragm of the valve is 1.0 mm.

TABLE IV
DESIGN ITERATIONS

PART	Layer height (μm)	Pump width (mm)	Diaphragm thickness (mm)	Hardness (Shore)
VALVE 1	25	24	1	27A
VALVE 2	25	28	1	27A
PISTON 1	25	24	1	27A
PISTON 2	25	24	1	50A
PISTON 3	25	28	0.9	50A
PISTON 4	16	28	0.9	50A

In the table, VALVE X refers to the valve block iteration X, and PISTON Y refers to the piston block iteration Y.

in-plane dimensions of the Si microfabricated MEMS pumps are 50 mm by 33 mm; also, the Si microfabricated MEMS pumps have a 20-mm diameter compression chamber, 4-mm diameter ports (pump inlet, outlet, and pneumatic actuation ports), and two 6.4 mm diameter valves. The 3-D printed pump design is significantly thicker than the pumps described in [3], [5] because (i) in the 3-D printed design the valves are placed on top of the compression chamber to save in-plane area, and (ii) the compression chamber of the 3-D printed pump has a 2.4 mm stroke versus the 6 μm stroke of the Si MEMS pumps.

Initially, the diaphragm pumps were entirely printed in the most flexible material of the TangoBlack® family, i.e., TangoBlack Plus® with a Shore hardness value of 27A, yielding mixed results. On the one hand, the valves printed in this material did not show signs of leaking or degradation after extensive testing; therefore, the design and constitutive material of the valves was not iterated throughout this study, only introducing variations of the frame that surrounds the valve set to match any iterations of the compression chamber (Table IV). On the other hand, the original compression chambers developed fractures at the root of the diaphragms at rather small number of cycles, which motivated an iterative optimization process of this component to extend its lifetime. In all of the iterations (i) the sidewalls of the compression chamber are bowed to minimize the dead volume upon compression, and (ii) the design incorporated fillets at the edges with the highest stresses. Four parameters of the compression chamber were varied in the optimization of this pump component (Table IV): hardness of the printable material, height of the printed layers, diaphragm thickness, and compression chamber

sidewall thickness (i.e., width of the frame). Based upon advice from Polyjet printing experts, the minimum thickness of the diaphragm was set close to 1.0 mm to avoid the risk of a leak across the membrane. The wider compression chamber assembly with the thinner diaphragm thickness printed with 16 μm thick individual layers in the Shore 50A TangoBlack® polymer yielded the best pumping performance and lifetime results.

The dimensions of the components of the pump were obtained by iterating the actual pump geometry (e.g., including diaphragm fillets) based on the results of axisymmetric finite element simulations using the commercial software Solidworks 2015 (Dassault Systemes, Waltham, MA). The finite element modeling effort focused on estimating the fundamental resonance frequency and the mechanical performance of the compression chamber, which is the slowest component of the pump, as well as the pump component that experiences the largest deformation and stresses. The use of finite element modeling was motivated by the non-linear nature of the physical problem; also, finite element modeling is an accepted engineering approach to accurately model structural problems with realistic geometries [35].

The deflection of a diaphragm can be modeled using linear deformation theory if the deflection of the membrane is less than about half its thickness [35]. However, when the deformation of the membrane is larger, the in-plane tensile stress is comparable (or larger) than the bending stresses, thereby increasing the plate stiffness. In such case, the non-linear differential equation that describes the displacement w of a circular, uniform membrane made of an isotropic, elastic, and linear material, with loads perpendicular to the surface of the membrane, constrained at its outer radius $r = a$, and attached to a central stiff piston of radius $r = b$ is [36]

$$\frac{d^3w}{dr^3} + \frac{1}{r}\frac{d^2w}{dr^2} - \frac{1}{r^2}\frac{dw}{dr} - \frac{N_r}{D}\frac{dw}{dr} = \frac{Q}{D}; \tag{1}$$

with boundary conditions

$$w\,(r = a) = 0, \frac{dw}{dr}\,(r = a) = 0, \frac{dw}{dr}\,(r = b) = 0; \tag{2}$$

where N_r is the in-plane tension load per unit of circumference, D is the flexural rigidity of the diaphragm, i.e.,

$$D = \frac{Et_d^3}{12\left(1 - \upsilon^2\right)}; \tag{3}$$

where E and υ are the Young's modulus and Poisson ratio of the material, t_d is the thickness of the diaphragm, and Q is the shear force per unit of length, given by

$$Q = \frac{F_{piston}}{2\pi \cdot r} - \frac{\Delta P\left(r^2 - b^2\right)}{2r} \tag{4}$$

where ΔP is the pressure difference across the membrane and F_{piston} is the force acting on the piston, i.e., $\pi \cdot \Delta P \cdot b^2$ if pneumatically actuated. There is no closed form solution of equation (1).

Four physical properties are required to model the pump: the Young's modulus, the Poisson ratio, the tensile strength σ_y, and the density of the material, ρ. The Young's modulus and Poisson's ratio used in the simulations were set at 0.76 MPa (see Section II.C) and 0.3 [37], respectively. The tensile strength values measured by others [28], [38] are within the range of typical tensile strength for the TangoBlack® family of polymers provided by the vendor (Stratasys, Eden Prairie, MN) [24]; the tensile strength used in this study was set at 1.9 MPa, which is the lower bound of the range provided by the vendor for the TangoBlack® blend with 50A Shore hardness. For the density of the material, the middle of the range provided by the vendor was adopted, i.e., 1.125 gr/cm^3 [24].

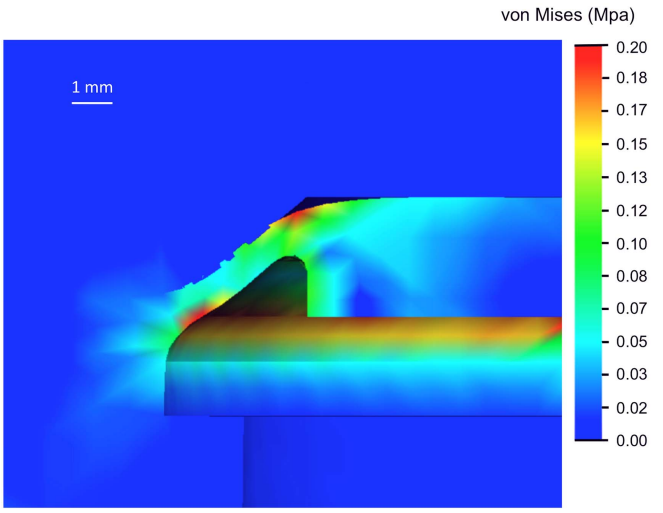

Fig. 7. Simulation results of the finite element stress analysis of the compression chamber piston in full actuation.

The fundamental resonance frequency f_r of a diaphragm with D_d diameter and t_d thickness is [39]

$$f_r = 2\pi\left(\frac{1.015}{D_d}\right)^2\sqrt{\frac{E \cdot t_d^2}{12\rho\left(1 - \nu^2\right)}}; \tag{5}$$

using $D_d = 20$ mm, $t_d = 0.9$ mm, and the values of the Young's modulus and Poisson values previously quoted, results in a natural frequency of the compression chamber equal to 114.6 Hz. Finite element simulations of the pump using the physical values previously quoted estimate at 106 Hz the natural frequency of the compression chamber, which is slightly faster than the actuation time of the solenoid valves of the experimental apparatus used to characterize the pump (see Section IV).

Fig. 7 shows a cross-section of the stress field solution (in MPa) of the static stress simulation of the piston. In the simulations, the displacement is set to the full stroke value of 2.4 mm. This is equivalent to a pressure of 27.4 kPa applied to the compression chamber piston and the 3.6 mm radial diaphragm area. The maximum stress is at the root of the diaphragm, i.e., the edge at which the diaphragm is attached to the compression chamber. The maximum stress is estimated at 0.20 MPa, which is well below the 1.9 MPa lower bound of the tensile strength of the material [24], [28]. The compression chamber was designed to allow for a maximum diaphragm elongation of 20%, which corresponds to the suggested maximum elongation to avoid failure by fatigue of the TangoBlack® Plus polymer [40].

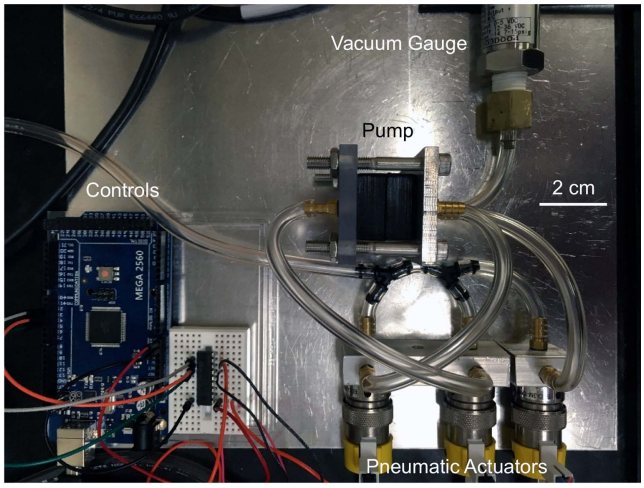

Fig. 8. Photograph of the experimental apparatus used to characterize the 3-D printed mini pumps.

IV. Apparatus and Experimental Procedure

The apparatus shown in Fig. 8 was used to characterize the 3-D printed pumps. A top aluminum plate and a bottom acrylic plate held the printed devices with nuts and bolts. The pump required to be compressed by 8% (2 mm) to prevent leakage at the plate/pump interfaces; unfortunately, this procedure has the collateral effect of reducing the displacement of the compression chamber piston and increasing the relative size of the pump dead volume. The acrylic plate has one threaded hole to accommodate a miniature brass fitting with an o-ring for actuation of the chamber piston. The clear acrylic plate is also used as a window to observe the extent of displacement of the piston as the N_2 supply pressure is varied to optimize the stroke.

The top plate has four threaded holes: the outer two for vacuum and exhaust ports, and the inner two for vacuum and exhaust valve actuation. Three-way solenoid valves (Clippard, model EC-3M-12-H) with a response time of 10 ms are used for valve and diaphragm pneumatic operation. Compressed nitrogen is fed to one side of the solenoid valves, vacuum to the other side, and ¼" Tygon tubing is plumbed from the barbed fittings on the plates to the solenoid valves. The vacuum is supplied by an Edwards nXDS15i scroll pump through 8 ft of NW25 bellows and 8 ft of ¼" tubing.

The pump exhausts to atmosphere and the vacuum port is plumbed to a pressure gauge with an accuracy of +/-15 Torr and a response time of 20 ms (Transducers direct, model TDH31, vacuum to 15 psi range). The effective vacuum chamber volume is 1 cm^3; this volume includes the pressure transducer volume, the pipework and fittings, and the printed vacuum valve volume. An Edwards Model 825 mass flow controller (MFC) with a maximum flow rate of 500 sccm was used in parallel with the pressure transducer plumbed to the vacuum port (not shown in Fig. 8) to measure flow rate versus pressure of the diaphragm pumps. The MFC was calibrated with an Omega Engineering Model FMA-5606, 0-500 sccm mass flow meter. Leak checks were conducted to make sure the pressure versus flow rate data reflected what was occurring inside the compression chamber.

TABLE V
Valve and Piston Timings

Frequency (Hz)	Vacuum valve close, Exhaust valve open (ms)	Piston up (ms)	Exhaust valve close, Vacuum valve open (ms)	Piston down (ms)
1.82	2, 10	263	2, 10	263
2.13	2, 10	223	2, 10	223
3.23	2, 10	143	2, 10	143
5.26	2, 10	83	2, 10	83

Also, for all of the data presented, the effective speed was calculated and was found less than the volumetric displacement of the compression chamber per second (the actuation frequency times the chamber volume, i.e., 1 cm^3).

The solenoid valves are controlled with an Arduino micro controller (Mega 2560) programmed to supply pressurized N_2 or vacuum to the pump valves and diaphragm. The pumping performance is optimized by adjusting the timing of the valves and N_2 pressure. Table V contains the sequencing and delay times used. During pump testing, a Dataq DI-149 datalogger collected voltage signals from the pressure transducer at a rate of 8 Hz. The piston and valves are activated pneumatically with pressurized nitrogen regulated to 15 psig and a vacuum supplied by an Edwards nXDS15i connected to the three-way solenoid valves. When a three-way solenoid valve is switched to either pressurized nitrogen or supplied vacuum, the valves and piston are either pushed forward or pulled back. Time between switching depends upon actuation frequency. Operating the pump at low frequencies (e.g., 1.82 Hz, 275 ms) results in much more time between switching compared to operating at high frequencies (e.g., 5.26 Hz, 95 ms), which allows more time for pressure to build or supply vacuum pressure to drop behind the membranes being actuated. This could result in less than full displacement of the compression chamber diaphragm at higher actuation frequencies and hence higher base pressures.

V. Experimental Results and Discussion

The printed devices consistently pumped down a 1 cm^3 volume from atmospheric pressure to 110 Torr in under 4 seconds while operating at 1.82 Hz (Fig. 9); the base pressure is a threefold improvement over our earlier results using a single-material printed pump [18] and represents a 33% reduction in the lowest base pressure reported for a miniature single-stage microfabricated diaphragm pump [5]; the base pressure also compares favorably with that of commercially available non-microfabricated miniature diaphragm pumps: the 2-stage diaphragm pump D27-D3k from TCS Micropumps has a base pressure of 340 Torr [41], the 2-stage diaphragm pump DP0110T from Nitto Kohki has a base pressure of 310 Torr [42], and the 1-stage diaphragm pump 1610VD DC FKM from Gardner Denver Thomas has a base pressure of 75 Torr [43]. Compared with our previous work, we attribute the improvement to a stronger vacuum used to actuate the valves, a lower actuation frequency, and a reduction in the compression of the pump by the plates from 17% to 8%. The pressure on

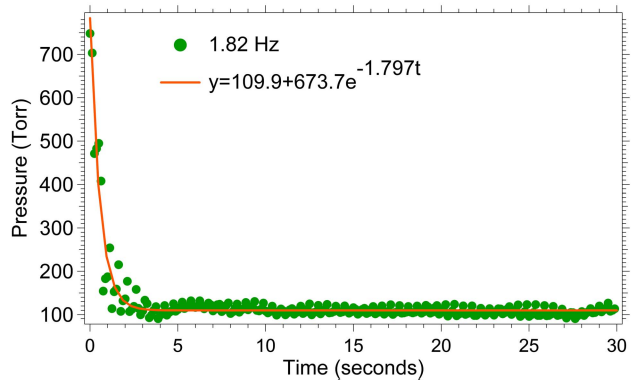

Fig. 9. Pressure versus time characteristic for devices composed of a Valve 2 assembly and Piston 4 assembly as described in Table IV. Data in green, exponential curve fit in orange with exponent S/V= 1.797 s^{-1}.

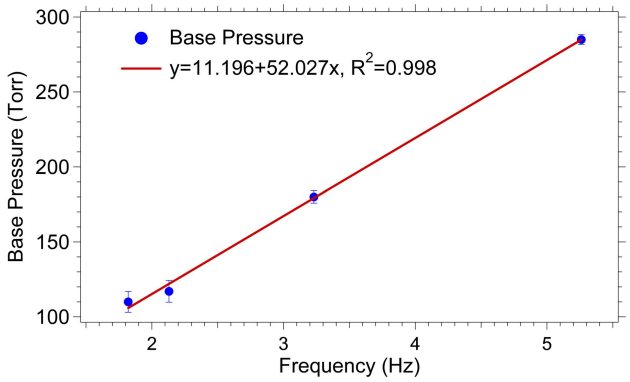

Fig. 10. Average base pressure (blue points) versus actuation frequency and linear fit of the data (red line) versus frequency. Pump base pressure rises as actuation frequency increases. The data were collected from pumps composed of a Valve 2 assembly and Piston 4 assembly as described in Table IV. The average base pressure at each frequency was calculated by taking the average of several hundred data points; error bars represent one standard deviation.

the compression chamber piston is measured with an inline Bourdon dial gauge between the regulated set point of 15 psig when not applied and about 8 psig (54.4 kPa) when applied during a pumping cycle. The applied pressure of 54.4 kPa is larger than the modeled pressure of 27.4 kPa required for full stroke displacement; the force exerted by the extra pressure is absorbed by the frame of the mechanism, which is far stiffer than the membrane.

In a diaphragm pump, the pressure p versus time t characteristic is an exponential decay given by [44]

$$p(t) = p_f + (p_o - p_f)\, e^{\left(-\frac{S}{V}t\right)}; \tag{6}$$

where $p(t \to \infty) = p_f$ is the base pressure, $p(t = 0) = p_o$ is the starting pressure (i.e., 1 atmosphere), V is the volume being pumped down, and S is the effective pumping speed; this reduced-order model is an idealization, that is, it assumes the pumping is done continuously instead of in a series of discrete events. The data shown in Fig 9 is satisfactorily described by an exponential decay fit with effective pumping speed equal to 1.797 cm^3/s (slightly less than the maximum speed of a 1 cm^3 volume actuated at a frequency of 1.82 Hz, i.e., 1.82 cm^3/s), p_f = 109.9 Torr, and $(p_o - p_f)$ = 673.7 Torr. The small offset of 23.6 Torr between the $(p_o - p_f)$ value from the fit and the actual value (650.1 Torr) may be accounted for in the measurement uncertainty of +/− 15 Torr of the pressure gauge and the scatter in the data points near the approach to p_f; the oscillatory behavior of the pressure-vs.-time characteristic in a positive displacement pump has also been reported by other researchers [45].

The base pressure of the pump improves as the frequency of actuation is lowered (Fig. 10), suggesting that the chamber compression is more complete when the pneumatics have longer time to actuate the diaphragm at the lower frequency. The 110 Torr base pressure is a single-stage compression ratio of 6.9:1 and is equivalent to a pump with a 14.5% dead volume. The base pressure as a function of the exhaust pressure p_e (i.e., 1 atmosphere) is

$$p_f = p_e \frac{V_d}{V_p} = p_e / compression\, ratio \tag{7}$$

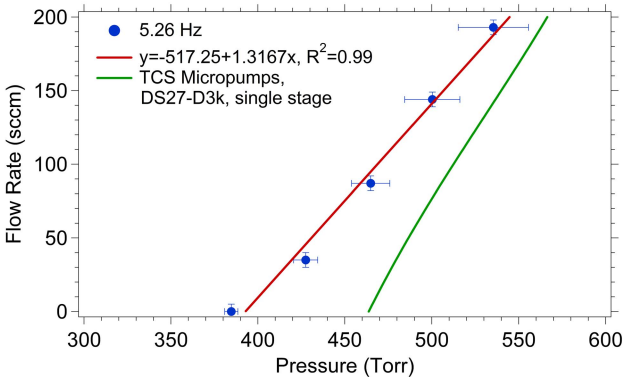

Fig. 11. Flow rate (blue points) versus average pressure and linear fit of the data versus average pressure (red line) while operating at 5.26 Hz along with published throughput data for a single-stage diaphragm pump from TSC Micropumps, model DS27-D3k (green line). The data were collected with a pump composed of a Valve 1 assembly and Piston 2 assembly as described in Table IV. Error bars on the pressure represent one standard deviation, and on the flow rate +/− 5 sccm.

where V_d and V_p are the dead volume and pump volume, respectively. Three tentative reasons are proposed to explain why the 3-D printed mini pumps did not achieve a base pressure of 38 Torr as predicted by equation (7) for a 5% dead volume. First, the compression chamber piston might not fully actuate each cycle –particularly on the back stroke, i.e., when the chamber piston is pulled down by the vacuum. Second, the compression chamber volume is reduced when the pump is compressed by 8% between the plates, while the dead volume does not significantly change because it does not make contact to the top or bottom surfaces of the pump; this would reduce the compression ratio to ∼18.4 and the base pressure would increase to ∼42 Torr. Third, it might be possible that the valves have internal leaks. The experimental apparatus should also be upgraded with a more precise pressure gauge to measure more accurately pressures below 100 Torr.

The mass flow rate of nitrogen versus pressure measured at diaphragm pump actuation frequency of 5.26 Hz is depicted in Fig. 11. Each data point in the plot is an average of about

TABLE VI
LONGEST COMPONENT LIFETIMES

PART	Slice height (μm)	Pump width (mm)	Diaphragm thickness (mm)	Lifetime (kilocycles)
VALVE 1	25	24	1	>1,000
VALVE 2	25	28	1	>2,300
PISTON 1	25	24	1	20
PISTON 2	25	24	1	108
PISTON 3	25	28	0.9	75
PISTON 4	16	28	0.9	>850

200 pressure readings at each flow rate, and the error bars represent +/- one standard deviation of the values. As the flow rate increases, the standard deviation of the average pressure measurements also increases. A representative result is a nitrogen flow rate of 200 sccm at 535 Torr; this flow rate is much higher than reported flow rates from any microfabricated diaphragm vacuum pump [5]–[7], and higher than those reported for a commercially available diaphragm pump of comparable dimensions made with standard manufacturing (green curve, Fig. 11 [41]).

As previously described in Section III, four parameters of the compression chamber were modified with the intention to attain longer lifetimes: (i) hardness of the printable material, (ii) height of the printed slices, (iii) diaphragm thickness, and (iv) compression chamber lateral wall thickness (i.e., width of the pump body). Table VI lists the largest number of actuation cycles measured before diaphragm failure for a given combination of parameters; the descriptions of the different components tested are shown in Table IV. With the improvements made to the design, compression chamber diaphragms exhibited lifetimes approaching 1 million cycles, while the valves membranes have not leaked after more than 2 million cycles. As predicted by the finite element simulations, the failed diaphragms show cracks at their root, which is the point of maximum stress. Changing the hardness of the compression chamber assembly from Shore 27A to 50A increased a fivefold the lifetime of the hardware; however, increasing the hardness to 70A (not shown on Table IV) resulted in a diaphragm too stiff for full actuation, and a significant reduction in lifetime. Therefore, it was assumed that the optimal hardness was around 50A and variation of other aspects of the pump was prioritized. The thickness of the lateral material surrounding the compression chamber was not equal on all sides in the 24 mm wide design (the lateral material was 2 mm thick on two opposite sides and 7.5 mm thick on the two other); during actuation it was noticed that the thinner 2 mm thick walls deformed. Increasing the width of the pump from 24 mm to 28 mm provided wall thicknesses of 4 mm and 7.5 mm, resulting in less deformation during actuation. During this iteration, the diaphragm thickness was also decreased from 1 mm to 0.9 mm to improve flexibility without causing leaks through the membrane. Printed in 25 μm thick layers, the design yielded shorter cycle lifetimes than the previous hardware iteration, but printed with 16 μm layers results in an order of magnitude increase in the lifetime, i.e., $>$850k cycles actuation prior to leakage. These results are very encouraging; however, it is important to point out that the reported exploration of the lifetime of the pumps is preliminary and further studies are required. Sometimes the combinations tested had visibly shorter lifetimes, probably due to print-to-print variation, damage of the device during removal of the sacrificial material that fills-in the internal cavities during printing, and/or assembly/disassembly of the devices.

A number of directions for further development of the miniature diaphragm pumps are identified. A first direction is the demonstration of cascaded systems, that is, a set of compression stages grouped in series with the objective to lower the base pressure delivered by the pump. With the demonstrated compression ratio of 6.9:1, it should be possible to reach a base pressure below 1 Torr, which is a low enough pressure to back a turbo-molecular pump for miniaturized mass spectrometry instruments [2] or to be the main pump in mid-resolution terahertz spectroscopy [46]. Having a multi-stage diaphragm pump system also helps reduce the power required in pumping by making the polytrophic coefficient of the compression closer to the isothermal limit [47] assuming there is no significant increase in power consumption from having a plurality of valves added to the hardware. Given the superior lifetime performance of the valves compared to the main piston, there is considerable merit in exploring pumping stages with smaller stroke, and looking closely at the piston/volume geometry to minimize stresses, exploiting on the freeform nature of AM processing.

A second possibility for further investigation is the development of passive valves to avoid the need to provide actuation to these components. However, the body of work on MEMS valves demonstrates that active valves have associated smaller leaks compared to passive valves [34], [48].

Third, a clear limitation of the current pump hardware is its actuation because it restricts the portability and deployability of the pumps. Furthermore, it is not physically possible to produce lower vacuum than the actuation vacuum, regardless of the nominal compression ratio of the chamber. A possibility is to integrate mesoscaled off-the-shelf actuators with the printed part; however, a more interesting direction is to investigate 3-D printed actuators. This exploration might imply a combination of printing methods because, besides being capable of processing selected flexible, sacrificial, and optically clear printable feedstock, the developers of polyjet printing hardware have focused on providing very fine control of the color of the printed part [17] instead of printing functional materials, e.g., structures that transduce stimuli. Transducing mechanisms compatible with long-stroke, large force actuation are of particular interest for this application, e.g., magnetic actuation. Researchers have recently demonstrated 3-D printing of permanent magnets using extrusion of thermoplastics doped with magnetic microparticles [49].

Finally, the issue of the variability of the physical properties of the printable material needs to be further investigated. The vendor of the printable feedstock specifies ranges for many of the physical properties of objects printed with their resins. The vendor is not clear on whether the variation occurs across different batches of the same resin, within the

same batch, if the spread is due to aging of the resin, etc. Control of the physical properties would be highly desirable for commercialization of the pump; otherwise, the designs might need to be conservative and use the lower bound values.

VI. Conclusion

The first demonstration of a multi-material, fully additively manufactured, miniature diaphragm pump for creation and maintenance of low vacuum from atmospheric conditions was reported. Using polyjet 3-D printing technology, a single-stage vacuum pump design with active valves that has a total pumping volume of 1 cm^3 with 5% dead volume was implemented. While operating at 1.82 Hz, the devices consistently pumped down from atmospheric pressure to 110 Torr in under 4 seconds, which is the smallest and fastest base pressure reported in the literature for a microfabricated diaphragm pump; the base pressure also compares favorably with commercial, non-microfabricated, miniature diaphragm vacuum pumps. In addition, the pumps can deliver mass flow rates as high as 200 sccm at 535 Torr, which is much higher than any of the reported flow rates from a diaphragm vacuum pump manufactured with standard microfabrication, and larger than the reported flow rates of a commercial, non-microfabricated, miniature diaphragm vacuum pump. The outgassing rate of the printable photopolymer used to make the pumps is on a par with vacuum compatible elastomers. Compression chamber diaphragms exhibited lifetimes approaching 1 million cycles, while the valve membranes have not leaked after over 2 million cycles. Tentative research directions include cascaded systems to lower the base pressure delivered by the pump, development of passive valves to simplify the actuation of the pumps, and development of 3-D printed long-stroke, large force actuators.

Acknowledgment

The authors would like to thank Anthony Keen, Edwards Vacuum, for the outgassing rate measurements, Ashley Beckwith and Zhumei Sun, Velasquez Research Group, Massachusetts Institute of Technology (MIT), for helping conduct metrology of printed structures, and Mitchell Hsing and Parker Gould, Schmidt Research Group, MIT, for their help with this project.

References

[1] A. Malcolm, S. Wright, R. R. A. Syms, N. Dash, M.-A. Schwab, and A. Finlay, "Miniature mass spectrometer systems based on a microengineered quadrupole filter," *Anal. Chem.*, vol. 82, no. 5, pp. 1751–1758, 2010.

[2] R. R. A. Syms and S. Wright, "MEMS mass spectrometers: The next wave of miniaturization," *J. Micromech. Microeng.*, vol. 26, no. 2, p. 023001, 2016.

[3] V. Sharma, "MEMS micropump for a micro gas analyzer," Ph.D. dissertation, Dept. Elect. Eng. Comp. Sci., Massachusetts Inst. Technol., Cambridge, MA, USA, 2009.

[4] K. Jousten, Ed., *Handbook of Vacuum Technology*, 1st ed. Hoboken, NJ, USA: Wiley, 2008.

[5] H. Zhou, H. Q. Li, V. Sharma, and M. A. Schmidt, "A single-stage micromachined vacuum pump achieving 164 torr absolute pressure," in *Proc. 24th Int. Conf. Micro Electro Mech. Syst. (MEMS)*, Cancún, Mexico, Jan. 2011, pp. 1095–1098.

[6] H. Kim, A. A. Astle, K. Najafi, L. P. Bernal, and P. D. Washabaugh, "A fully integrated high-efficiency peristaltic 18-stage gas micropump with active microvalves," in *Proc. IEEE 20th Int. Conf. Micro Electro Mech. Syst. (MEMS)*, Jan. 2007, pp. 131–134.

[7] A. Besharatian, K. Kumar, R. L. Peterson, L. P. Bernal, and K. Najafi, "Valve-only pumping in mechanical gas micropumps," in *Proc. IEEE 26th Microelectromech. Syst. Conf. (MEMS)*, Jun. 2013, pp. 2640–2643.

[8] M. Vaezi, H. Seitz, and S. Yang, "A review on 3D micro-additive manufacturing technologies," *Int. J. Adv. Manuf. Technol.*, vol. 67, nos. 5–8, pp. 1721–1754, Jul. 2013.

[9] S. Waheed *et al.*, "3D printed microfluidic devices: Enablers and barriers," *Lab Chip*, vol. 16, no. 11, pp. 1993–2013, Jun. 2016.

[10] A. K. Au, W. Huynh, L. F. Horowitz, and A. Folch, "3D-printed microfluidics," *Angew. Chem. Int.*, vol. 55, no. 12, pp. 3862–3881, 2016.

[11] L. F. Velásquez-García, "SLA 3-D printed arrays of miniaturized, internally fed, polymer electrospray emitters," *J. Microelectromech. Syst.*, vol. 24, no. 6, pp. 2117–2127, Dec. 2015.

[12] H. Gong, A. T. Woolley, and G. P. Nordin, "High density 3D printed microfluidic valves, pumps, and multiplexers," *Lab Chip*, vol. 16, no. 13, pp. 2450–2458, 2016.

[13] E. García-López, D. Olvera-Trejo, and L. F. Velásquez-García, "3-D printed multiplexed electrospinning sources for large-scale production of aligned nanofiber mats with small diameter spread," *Nanotechnology*, vol. 28, 2017.

[14] A. P. Taylor and L. F. Velásquez-García, "Electrospray-printed nanostructured graphene oxide gas sensors," *Nanotechnology*, vol. 26, no. 50, p. 505301, 2015.

[15] D. Olvera-Trejo and L. F. Velásquez-García, "Additively manufactured MEMS multiplexed coaxial electrospray sources for high-throughput, uniform generation of core–shell microparticles," *Lab Chip*, vol. 16, no. 21, pp. 4121–4132, 2016.

[16] *Polyjet*. Accessed: Aug. 18, 2017. [Online]. Available: https://www.stratasysdirect.com/solutions/polyjet/

[17] *Polyjet Materials*. Accessed: Aug. 18, 2017. [Online]. Available: https://www.stratasysdirect.com/materials/polyjet/

[18] A. P. Taylor and L. F. Velásquez-García, "3-D printed miniaturized diaphragm vacuum pump," in *Proc. IEEE 30th Int. Conf. Micro Electro Mech. Syst. (MEMS)*, Las Vegas, NV, USA, Jan. 2017, pp. 1292–1295.

[19] V. A. Lifton, G. Lifton, and S. Simon, "Options for additive rapid prototyping methods (3D printing) in MEMS technology," *Rapid Prototyping J.*, vol. 20, no. 5, pp. 403–412, 2014.

[20] B. P. Conner *et al.*, "Making sense of 3-D printing: Creating a map of additive manufacturing products and services," *Additive Manuf.*, vols. 1–4, pp. 64–76, Oct. 2014.

[21] *NinjaFlex*. Accessed: Aug. 18, 2017 [Online]. Available: https://ninjatek.com/products/filaments/ninjaflex/

[22] *Formlabs FLFLGR02 Material Properties*. Accessed: Aug. 18, 2017. [Online]. Available: https://formlabs.com/media/upload/Flexible-DataSheet_D93ECMO.pdf

[23] *Polyjet Materials Properties*. Accessed: Aug. 18, 2017. [Online]. Available: http://global72.stratasys.com/~/media/Main/Files/Material_Spec_Sheets/MSS_PJ_PJMaterialsDataSheet.ashx

[24] *Polyjet Flex & Polyjet Over-Mold Materials Specifications*. Accessed: Aug. 18, 2017. [Online]. Available: https://www.stratasysdirect.com/wpcontent/themes/stratasysdirect/files/materialdatasheets/polyjet/PolyJet_Flex_PolyJet_Overmold_Material_Specifications.pdf

[25] *Geometrical Product Specifications (GPS)—Surface Texture: Profile Method—Terms, Definitions and Surface Texture Parameters*, document ISO 4287:1997, accessed: Aug. 18, 2017. [Online]. Available: https://www.iso.org/standard/10132.html

[26] *Geometrical Product Specifications (GPS)—Surface Texture: Profile Method—Rules and Procedures for the Assessment of Surface Texture*, document ISO 4288:1996, accessed: Aug. 18, 2017. [Online]. Available: https://www.iso.org/standard/2096.html

[27] J. Scheibert, S. Leurent, A. Prevost, and G. Debrégeas, "The role of fingerprints in the coding of tactile information probed with a biomimetic sensor," *Science*, vol. 323, no. 5920, pp. 1503–1506, 2009.

[28] A. S. Dalaq, D. W. Abueidda, and R. K. A. Al-Rub, "Mechanical properties of 3D printed Interpenetrating phase composites with novel architectured 3D solid-sheet reinforcements," *Compos., A Appl. Sci. Manuf.*, vol. 84, pp. 266–280, May 2016.

[29] R. N. Peacock, "Practical selection of elastomer materials for vacuum seals," *J. Vac. Sci. Technol.*, vol. 17, no. 1, pp. 330–336, 1980.

[30] I. Chakraborty, W. C. Tang, D. P. Bame, and T. K. Tang, "MEMS microvalve for space applications," *Sens. Actuators A, Phys.*, vol. 83, nos. 1–3, pp. 188–193, 2000.

[31] H. Jerman, "Electrically activated normally closed diaphragm valves," *J. Micromech. Microeng.*, vol. 4, no. 4, pp. 210–215, 1994.
[32] L. Yobas, M. A. Huff, F. J. Lisy, and D. M. Durand, "A novel bulk micromachined electrostatic microvalve with a curved-compliant structure applicable for a pneumatic tactile display," *J. Microelectromech. Syst.*, vol. 10, no. 2, pp. 187–196, Jun. 2001.
[33] M. C. Carrozza, N. Croce, B. Magnani, and P. Dario, "A piezoelectric-driven stereolithography-fabricated micropump," *J. Micromech. Microeng.*, vol. 5, no. 2, pp. 177–179, 1995.
[34] D. J. Laser and J. G. Santiago, "A review of micropumps," *J. Micromech. Microeng.*, vol. 14, no. 6, pp. R35–R64, 2004.
[35] W. C. Young and R. G. Budynas, *Roark's Formulas for Stress and Strain*, 7th ed. New York, NY, USA: McGraw-Hill, 2002, ch. 5.
[36] D. C. Roberts, "Design, modeling, fabrication and testing of a piezoelectric microvalve for high pressure, high frequency hydraulic applications," Ph.D. dissertation, Dept. Mech. Eng., Mass. Inst. Technol., Cambridge, MA, USA, 2002.
[37] R. Critchley, I. Corni, J. A. Wharton, F. C. Walsh, R. J. K. Wood, and K. R. Stokes, "The preparation of auxetic foams by three-dimensional printing and their characteristics," *Adv. Eng. Mater.*, vol. 15, no. 10, pp. 980–985, 2013.
[38] I. Vu, L. Bass, N. Meisel, B. Orler, C. B. Williams, and D. A. Dillard, "Characterization of multi-material interfaces in polyjet additive manufacturing," in *Proc. 26th Annu. Int. Solid Freeform Fabrication Symp. (SFF)*, Austin, TX, USA, 2015, pp. 959–982.
[39] M. Géradin and D. Rixen, *Mechanical Vibrations: Theory and Application to Structural Dynamics*, 2nd ed. Hoboken, NJ, USA: Wiley, 1997.
[40] J. P. Moore and C. B. Williams, "Fatigue characterization of 3D printed elastomer material," in *Proc. 23rd Annu. Int. Solid Freeform Fabrication Symp. (SFF)*, Austin, TX, USA, 2012, pp. 641–655.
[41] *TCS Micropumps D3K Series Miniature Diaphragm Gas/Air Pump—Data Sheet*. Accessed: Aug. 18, 2017. [Online]. Available: http://www.micropumps.co.uk/DATA/pdf/DS27%20-%20D3k%20Data%20Sheet%20rev%201.pdf
[42] *Nitto Diaphragm Pump Lk053_DP0110T*. Accessed: Aug. 18, 2017. [Online]. Available: https://www.nitto-kohki.co.jp/e/prd/new/pdf/Lk053_DP0110T.pdf
[43] *Gardner Denver Thomas Mini Diaphragm Pumps Models 16xx*. Accessed: Aug. 18, 2017. [Online]. Available: https://www.gd-thomas.com/assets/0/121/142/134/336/79a05467-b45d-4512-95dc-f97aa87fec5c.pdf
[44] J. F. O'Hanlon, *A User's Guide to Vacuum Technology*, 3rd ed. Hoboken, NJ, USA: Wiley, 2003, p. 360.
[45] R. Frey and J. Dual, "Modelling and experimental characterization of diaphragm pumps and tubing," in *24th Int. Congr. Theor. Appl. Mech. Tech. Dig.*, Montréal, QC, Canada, 2016, p. 2.
[46] S. Nagarajan, C. F. Neese, and F. C. De Lucia, "Cavity-based medium resolution spectroscopy (CBMRS) in the THz: A bridge between high- and low-resolution techniques for sensor and spectroscopy applications," *IEEE Trans. THz Sci. Technol.*, vol. 7, no. 3, pp. 233–243, May 2017, doi: 10.1109/TTHZ.2017.2680841.
[47] J. R. Simões-Moreira, "Fundamentals of thermodynamics applied to thermal power plants," in *Thermal Power Plant Performance Analysis*. New York, NY, USA: Springer, 2012, pp. 7–39.
[48] K. W. Oh and C. H. Ahn, "A review of microvalves," *J. Micromech. Microeng.*, vol. 16, no. 5, pp. R13–R39, 2006.
[49] C. Huber *et al.*, "3D print of polymer bonded rare-earth magnets, and 3D magnetic field scanning with an end-user 3D printer," *Appl. Phys. Lett.*, vol. 109, no. 16, p. 162401, 2016.

Anthony P. Taylor received the B.Sc. degree (*cum laude*) from Saint Lawrence University, Canton, NY, in 1985; the M.S. degree from the University of Arizona, Tucson, AZ, in 1988; and the Ph.D. from Rensselaer Polytechnic Institute, Troy, NY, in 1993, all in physics.

He has been with Edwards Vacuum, Sanborn, NY, as an Applications Engineer and Applications Technologist. He has also been a Visiting Scientist with the Velásquez–García Group, Massachusetts Institute of Technology, since 2014. His research with MIT has focused on novel fabrication methods of micro and nanosystems, specifically electrospray-printed gas sensors for vacuum and gas abatement applications, and more recently on 3-D-printed miniature vacuum pumps.

Luis Fernando Velásquez-García (M'09–SM'10) received the (*magna cum laude*) degrees (valedictorian) in mechanical engineering and civil engineering from the School of Engineering, Universidad de Los Andes, Bogotá, Colombia, in 1998 and 1999, respectively, and the M.S. and Ph.D. degrees from the Massachusetts Institute of Technology (MIT), Cambridge, MA, USA, in 2001 and 2004, respectively.

In 2004, he became a Post-doctoral Associate with the Microsystems Technology Laboratories, MIT, where he was appointed as a Research Scientist in 2005. Since 2009, he has been a Principal Scientist and Core Member of MTL. He is an expert in micro and nanofabrication technologies. He leads a group that conducts research on micro and nanoenabled multiplexed scaled-down systems for space, energy, healthcare, manufacturing, and analytical applications that exploit high-electric field phenomena, e.g., electrospray, gas ionization, field emission, X-rays, and plasmas. He has authored over 40 journal publications and 60 conference proceedings publications, and holds 15 patents on MEMS/NEMS technologies. His research currently focuses on additively manufactured micro and nanosystems.

Dr. Velásquez-García is a full member of Sigma Xi and a Senior Member of the American Institute of Aeronautics and Astronautics. He served as the Co-Chair of the 15th International Conference on Micro and Nanotechnology for Power Generation and Energy Conversion Applications (PowerMEMS 2015).